JOTCS A
Journal of the Turkish Chemical Society Section: A Chemistry
TURKISH CHEMICAL SOCIETY

Fabrication of Textile-Based Flexible Supercapacitor with a Textile Dye on Polyaniline-Based Composite Electrode for Enhanced Energy Storage

Sibel Yazar

Istanbul University-Cerrahpasa, Engineering Faculty, Department of Chemistry, 34320 Avcilar, Istanbul, Turkey

Abstract: Polyaniline (PANI) is a promising conductive polymer for use in energy storage applications. Here, a one-step hydrothermal method of PANI polymerization on carbon felt electrode was synthesized using an azo dye, a bisulfonated dichloro anionic dye molecule to enhance an efficient textile-based flexible supercapacitor electrode material for energy storage applications. The electrode material synthesized at concentration of 2 mM AY17 exhibits 814.1 F g^{-1} at the scan rate of 5 mV s^{-1} with multiwall carbon nanotubes (MWCNTs). Due to electrostatic interaction with the polymer, the presence of high electronegativity Cl atoms in the dye molecule significantly improves the PANI structure's electron donor/acceptor properties. A symmetric supercapacitor exhibits an energy density of 11.7 W h kg^{-1} at a power density of 300 W kg^{-1}, and it is 4.5 W h kg^{-1} at 1800 W kg^{-1} in 3.0 M KCl aqueous electrolyte. The capacitance retention performance value of the symmetric supercapacitor exhibited 81.76% after 2500 cycles.

Keywords: Polyaniline, textile dye, hydrothermal synthesis, flexible electrode, supercapacitor.

Submitted: June 07, 2022. **Accepted:** October 03 ,2022.

Cite this: Yazar S. Fabrication of Textile-Based Flexible Supercapacitor with a Textile Dye on Polyaniline-Based Composite Electrode for Enhanced Energy Storage. JOTCSA. 2022;9(4):1295–308.

DOI: https://doi.org/10.18596/jotcsa.1127200.

***Corresponding author. E-mail:** sibelyazar@iuc.edu.tr.

INTRODUCTION

The fast charge/discharge capabilities and high energy-power density of supercapacitors are good alternatives for energy storage devices (1). Electric double-layer capacitors, pseudocapacitors, and hybrid capacitors with both can be classified based on their energy storage system (2). In pseudocapacitors, a redox process occurs to store the charge, while in EDLCs, charges are electrostatically accumulated at the electrode/electrolyte interface (3). In hybrid supercapacitors, these two events co-occur on the electrode surface. Pseudocapacitors are commonly made of conductive polymers (CPs), and transition metal oxides/hydroxides (4). Carbonous materials is frequently used for EDLCs (5). Carbon-based materials or additives with redox behavior can be used to achieve high specific capacitance and long-cycling life for electrode materials (6).

PANI has unique properties in conducting polymers and easy polymerization. It has attracted some applications such as sensors, electronic devices, corrosion inhibitive materials, energy storage materials, and photonic devices (7). The polymerization of PANI, the aniline monomer exists in one of three oxidation states: leukoemeraldine, emerald, and pernigranilin. The fully oxidized form of PANI is known as pernigranilin. The totally reduced form of PANI is known as lecomeraldine, and half of the oxidized PANI is reduced to emerald (8). The physical/chemical properties of PANI-based supercapacitors can be significantly improved by doping process, and there are many studies combining carbon nanotubes and

carbonaceous materials such as graphene for their use in supercapacitors (9–11). The various compounds are utilized as dopants in supercapacitor electrodes as redox active chemicals, resulting in higher specific capacitance and energy density. Furthermore, when the conductive polymer structure is doped with large anions, since the polymer is immobile in the matrix, small electrolyte cations are involved in the charging/discharging process without large volume changes. Thus, the cyclic stability of the polymers is improved (3). The strong contact between the functional groups of the dye molecules as a counterion and the PANI improves capacitance performance (12). Dye molecules' anionic sulfonic groups interact electrostatically with the positively charged polymer structure. When previous research is examined, there are very few supercapacitor studies that have been studied with dye molecules. Q. F. Lu et al., reported the capacitance value of 579 F/g a dye-functional graphene/PANI (rGAP) electrode at the current density of 0.5 A/g in 1 M H_2SO_4 electrolyte solution. It has also been reported that 75% of the capacitance retention after 2000 cycles (13). With Alizarin Red S dye, Quanlu Wang et al. achieved a capacitance value of 461 F/g at 0.5 A/g current density (14). PANI doped with Prussion blue supercapacitor electrode was successfully constructed by Y. Xueying et al., that reported a specific capacitance of 218.4 F/g at a current density of 5 A/g. After 2000 cycles, they discovered that it had retained 94 percent of its capacitance (15).

The dyes used as energy storage materials in previous studies generally contain metals with redox behavior consisting of ring structures that provides electron delocalization, and also molecules with the highest degree of dissociation, such as sulfonic acid groups, are beneficial. Here, acid yellow 17 (AY17), because of the functional groups and the ring structures, assists the electron delocalization and improves the capacitance performance of the electrode materials. Furthermore, the inclusion of strong electronegativity of Cl atoms in the dye molecule, which is in electrostatic contact with the polymer, considerably enhances the electron donor/acceptor characteristics of the PANI structure (16).

In this study, an energy storage material of textile-based flexible electrode with a textile dye on multi-walled carbon nanotubes/polyaniline composite has been developed. PANI/MWCNT was synthesized on a carbon cloth electrode as a current collector in the presence of Acid Yellow 17 (AY17) counterion carrying an anionic sulfonate group. Disodium 2,5-dichloro-4-(5-hydroxy-3-methyl-4-(sulfophenylazo) pyrazol-1-yl) benzenesulfonate, namely acid yellow 17, is one of the basic color dyes, textile, paper, paint, pharmaceutical cosmetics and cleaning materials such as detergent, soap (17). Cyclic voltammetry, galvanostatic charge/discharge, and electrochemical impedance spectroscopy experiments were used to investigate the influence of the electrochemical performance of PANI/MWCNT/AY-13(3mM) as supercapacitor electrode in half-cell and full-cell applications.

EXPERIMENTAL

Materials

Carbon nanotube (multi-walled, 50-90 nm diameter, >95% carbon basis) and Acid Yellow 17 were purchased from Sigma-Aldrich. Aniline, $FeCl_3.6H_2O$, HCl, ethanol (CH_2OH), nitric acid (HNO_3,%65), potassium chloride (KCl), and acetone were purchased from Merck Schuchardt OHG (Hogenbrunn, Germany). Carbon felt (Cft) was provided by Mersen Istanbul Industrial Products Inc.

Synthesis of AY17 modified PANI/MWCNTs

To remove impurities on the electrode surface, carbon felt electrodes were washed with acetone in an ultrasonic bath for 40 minutes and then dried at room temperature overnight. After that, it was soaked in HNO_3 and stored at ambient temperature for 72 hours. The treated carbon felt electrodes were rinsed in distilled water until they reached a neutral pH, then dried in a 40 °C oven. Hydrothermal synthesis was used to make polyaniline/multi-walled carbon nanotubes (PANI/MWCNTs). After ultrasonically adding 50 mg MWCNTs to 100 mL of 1.0 M HCl aqueous solution for 1 hour at room temperature, 10 mmol aniline was added to the solution. As an oxidant, 25 mmol $FeCl_3.6H_2O$ was added to the aforementioned solution (18,19). The prepared homogeneous solution and 4.0 × 5.0 cm^2 carbon felt electrode was added to the autoclave for hydrothermal synthesis for six h at 120 ºC (20). The electrodes were then rinsed in 1.0 M HCl solution and distilled water, then dried for 24 hours at 40 °C. The effect of counter ion concentration on the supercapacitor electrode was investigated in the presence of 1.0, 2.0, 3.0, 4.0, and 5.0 mM AY17 (see Table 1). PANI/MWCNTs were synthesized with 0.5 mg/L MWCNTs, and the remainder of the methods were the same as for PANI.

Characterization

The microstructure of the sample pictures of the electrode surface was examined using a Zeiss EVO® LS 10 (SEM) instrument (USA). Bruker Al-pha-T DRIFT spectrometer with 30° reflection ac-cessory (M112-06/08) was used to investigate the chemical structure of electrode material. A SII6000 Exstar TG/DTA 6300 apparatus was used to per-

form thermogravimetric analysis (TGA) of electrode materials. The phase and crystallinity of the samples were determined using the XRD pattern of the materials (XRD, PANalytical X'Pert PRO Cu at 45 kV).

The surface area and pore size volume parameters were calculated using the BET analysis (Quantachrome Instruments, USA). The active mass coated on the carbon felt electrode was measured with a balance (Radwag) with an accuracy of 0.01 mg before and after hydrothermal synthesis. The active substance was coated onto carbon felt at a quantity of 3.0 mg cm^{-2}.

Table 1. The ratio of raw materials used in supercapacitor electrode samples.

Sample	MWCNT (mg/L)	ANI (mmol)	AY17 (mM)
PANI	-	10.0	-
PANI/AY17	-	10.0	3.0
PANI/MWCNTs	0.5	10.0	-
PANI/MWCNTs/AY17-1	0.5	10.0	1.0
PANI/MWCNTs/AY17-2	0.5	10.0	2.0
PANI/MWCNTs/AY17-3	0.5	10.0	3.0
PANI/MWCNTs/AY17-4	0.5	10.0	4.0
PANI/MWCNTs/AY17-5	0.5	10.0	5.0

Electrochemical measurements

At room temperature, the electrochemical measurements of the acquired samples for the half-cell electrode system and the symmetric supercapacitor device (full-cell system) were performed using an Ivium Vertex Instruments Potentiostat/Galvanostat (Ivium Technologies B.V, The Netherlands). The reference electrode and counter electrode for the half-cell system were the Silver/Silver chloride (Ag/AgCl) electrode and Pt wire, respectively. The working electrode was a carbon felt electrode coated with an active substance.

The electrolyte was a 3.0 M KCl aqueous solution. At room temperature (252°C), the electrochemical characterizations were performed using cyclic voltammetry (CV) at various scan rates, galvanostatic charge/discharge test (GCD) at varied current densities, and electrochemical impedance spectroscopy (EIS) between 0.01-10,000 Hz. Equations (1) and (2) were used to compute the specific capacitance (C, F g^{-1}) of the electrodes based on the CV and GCD curves, respectively (21,22):

$$C=\frac{1}{mv\left(V_2-V_1\right)}\int_{V_1}^{V_2} I\left(V\right)dV \qquad (1)$$

$$C=\frac{I\,\Delta t}{m\Delta V} \qquad (2)$$

where m is the mass of electroactive material; V_1 and V_2 are the cathodic and anodic voltage, respectively. The integral is calculated from the encircled area by cyclic voltammogram for a given scan rate v, ΔV and Δt are the operating potential and the discharge time by GCD curve, respectively.

The active material for the flexible supercapacitor electrode was inserted into the carbon felt (1x1 cm^2). The sandwich form of supercapacitor was created by combining two identical flexible electrodes. A symmetric supercapacitor was also created utilizing a 1.0x1.0 cm^2 piece of filter paper wetted with 3.0 M KCl as a separator. The following formulas can be used to compute the energy density (E) and power density (P) of a half-cell system (6,23):

$$E = \frac{C\times(\Delta V)^2}{2\times4\times3.6} \qquad (3)$$

$$P=\frac{3600\times E}{\Delta t} \qquad (4)$$

where C is the specific capacitance (F g^{-1}), ΔV, and Δt are the operating potential and discharge time during discharge of the device, respectively.

RESULTS AND DISCUSSION

Material Analysis

Figure 1a shows the FTIR spectra of PANI PANI/AY17, PANI/MWCNTs, and PANI/MWCNT/AY17-3 composite electrode material. All of the spectra's primary peaks revealed the characteristic PANI structural bands. The typical vibration peak of PANI was found in the FTIR spectrum at 3374 cm^{-1} for N–H stretching, 1563 cm^{-1} for C C stretching (quinoid rings), 1464 cm^{-1} for C C stretching (benzenoid rings), 1292 cm^{-}

[1] for C–N stretching (quinoid rings), and 1234 cm^{-1} for C–N stretching (benzenoid rings). The quinoid peak was a typical peak of electrical transport because it measured the degree of delocalization of electrons in the structure. The peaks at 1563 cm^{-1} and 1292 cm^{-1} gradually migrated to lower wave numbers (1559 cm^{-1}, 1232 cm^{-1}) in the PANI/AY17 spectra, with a noticeable increase in the intensity ratio of the quinoid to benzenoid ring peaks. When the materials, including MWCNTs in PANI/MWCNTs and PANI/MWCNTs/AY17-3 composite materials, were tested, the intensities of these peaks were shown to rise. Because of the oxidation effect of MWCNTs introduced to the media, interactions between PANI and carbon nanotubes may occur (24). In the spectrum of PANI/MWCNTs/AY17-3, the effect of acid yellow 17 on aniline polymerization was clearly seen. The asymmetric and symmetric stretching vibrations of the –SO3 groups were attributed to the peaks at 1118 and 1040 cm^{-1}, respectively (17). For PANI, PANI/AY17, PANI/MWCNTs, and PANI/MWCNT/AY17-3, a strong band was observed at 1069, 1106, 1117, and 1118 cm^{-1}, which was attributed to N=Q=N (Q, quinoid ring) (25). This strong peak also showed peaks at 1096 and 1040 cm^{-1} after doping with AY17. There would be an interaction of AY17 with quinoid diamine groups from PANI.

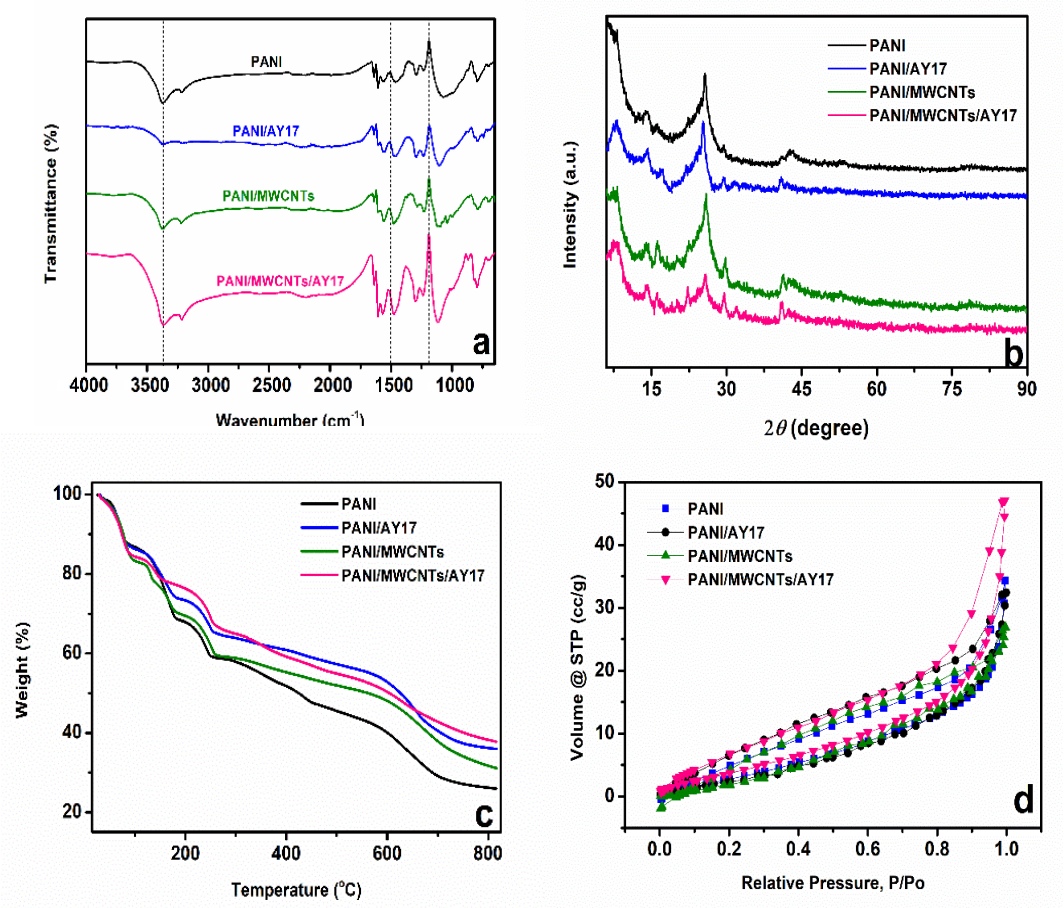

Figure 1: a) FTIR analysis, b) XRD patterns, c) TGA curves, and d) N_2 adsorption-desorption isotherms of PANI PANI/AY17, PANI/MWCNTs, PANI/MWCNT/AY17-3 composite electrode material.

Figure 1b shows the XRD analysis of PANI, PANI/AY17, PANI/MWCNTs, and PANI/MWCNT/AY17-3. The semi-crystalline polyaniline revealed three strong peaks at distinct diffraction angles, corresponding to crystal planes 121, 113, and 322 in Figure 1b, indicating that the majority of the chains structure of the resultant PANI was orientated in these three crystal planes (26). The PANI emeraldine salt showed a high peak at 2 = 25.57°, with a minor shoulder at 2 =

15 and 21, corresponding to the (322), (121), and (113) planes (27). PANI's XRD peaks showed a broad band around 25.57°, which was in good agreement with the literature. At 2 = 25.57°, PANI/AY17 showed a powerful and sharp peak. The crystal peaks for PANI/AY17 and PANI/MWCNTs were similar to those for PANI, showing that the PANI structure did not gain any additional crystalline structure. PANI/MWCNTs/AY17-3 XRD peaks were around 25.66°. In the case of composites, it was discovered that the PANI unit structure is intact, and peaks form around the peak shown in Figure 1b (28). The peaks of the PANI and the PANI/MWCNTs/AY17-3 nanocomposite were quite similar, indicating significant coverage of AY17-doped PANI onto MWNTs substrates (27). The MWCNTs also induced packing of the polymerization axis, thus maintaining a crystalline arrangement similar to that of PANI in the resulting composite (29).

Figure 1c represents the TGA thermograms of PANI, PANI/AY17, PANI/MWCNTs and PANI/MWCNT/AY17-3, which were performed under a nitrogen atmosphere. As seen in **Figure 1c**, the samples showed weight loss in three main stages; The elimination of moisture absorbed at the surface and polymer lattices was linked to the weight reduction in the first step (30). At 83.5 °C, PANI lost weight, while PANI/MWCNT/AY17-3 lost weight at 101.1 °C. Due to the elimination of counter ion, the TGA curve for PANI drops drastically compared to PANI/MWCNT/AY17-3 (a weight loss of 6.5%), and the amount by weight was 19.65% in the second phase, and the polymer itself began to degrade (31,32). Finally, at the end of the third step, a polymer weight loss of 25.94% was observed for PANI at 815 °C and was higher than PANI/MWCNT/AY17-3 (37.78% at 816 °C). While PANI degrades at a faster rate with temperature, PANI/AY17, PANI/MWCNTs, and PANI/MWCNT/AY17-3 samples were observed to be more thermally stable. Because of the interaction of PANI with MWCNTs and AY17 dye molecules, the thermal stability of the PANI/MWCNT/AY17-3 sample was increased compared to pure PANI, as demonstrated by FTIR and XRD tests.

The effect of MWCNTs and AY17 dopant on the porosity and specific surface areas of the composite on PANI was examined by BET analysis, as shown in Figure 1d. The specific surface areas for PANI and the PANI/MWCNT/AY17-3 composite were 18.29 and 25.77 m^2/g, respectively, according to the BET study. The PANI electrode had a pore volume of 0.042 cc/g, whereas the PANI/MWCNT/AY17-3 composite electrode had a pore volume of 0.070 cc/g, and all electrodes were given in Table 2. In energy storage devices, increasing the surface area and pore volume allows redox active chemicals in the electrolyte seeping from the pore volumes to interact more with the electrode surface, allowing for easier mass transfer and thus improved energy and power density (33).

Table 2: BET surface analysis of PANI, PANI/AY17, PANI/MWCNTs, and PANI/MWCNT/AY17-3 Electrodes.

Electrode materials	PANI	PANI/AY17	PANI/MWCNTs	PANI/MWCNT/AY17
Surface area/m^2/g	18.29	18.56	24.195	25.77
Pore volume/cc/g	0.042	0.048	0.040	0.072

Figure 2 depicts the surface morphology found in SEM images (a-d). The electrode surface was successfully coated with polymer by hydrothermal synthesis, and PANI gathered on the surface in cluster shapes. The polymer appears to be dispersed on the surface of the fibers in **Figures 2a and 2b** dispersed on the carbon felt for the PANI and PANI/AY17 electrodes. In the polymerization of PANI/MWCNT/AY17-3 on carbon felt medium, polymers with a larger porous feature and more compact structures were synthesized. A continuous matrix was also developed, which enhances the porosity of the composite and provides a large surface area for good electrode/electrolyte interface contact. This effect could indicate that carbon nanotubes interact with MWCNTs, allowing for improved PANI deposition (34). In Figure 2d, it can also be shown that adding AY17 to the PANI and MWCNT medium reduces the development of huge agglomerated polymerized islands with unfavorable growth. Because the electrode-electrolyte interaction was stronger on such active surfaces, more electrolyte ions may move during charge-discharge operations in energy storage devices (35).

Electrochemical Analysis

Using cyclic voltammetry, galvanostatic charge–discharge, and electrochemical impedance techniques, the reversibility and redox

electrochemical properties of PANI and its composite with multi-wall carbon nanotubes and acid yellow 17 as a counter ion were investigated. Using a half-cell system in 3.0 M KCl electrolyte solution, the effect of AY17 concentration on electrode capacitive performance was investigated in the range of 1 to 5 mmol/L AY17. The cyclic voltammograms, galvanostatic charge-discharge tests, and capacitance values calculated from these tests, as well as electrochemical impedance measurements, are shown in **Figure 3(a-i).** PANI, PANI/AY17, PANI/MWCNTs, and PANI/MWCNT/AY17-3 were analyzed with the applied potential in the range of −0.8-0.5 V in **Figure 3a**. **Figure 3a** shows the voltammogram following the sequence PANI/MWCNT/AY17-3 > PANI/MWCNTs > PANI/AY17> PANI at a scan rate of 100 mV s^{-1} versus Ag/AgCl reference electrode. It can be noted that the PANI/MWCNT/AY17-3 and PANI/MWCNTs composite CV have larger areas of the encircled areas. The galvanostatic charge–discharge tests were recorded in a potential window of −0.8-0.5 V at the current density of 8.3 A g^{-1}. In **Figure 3b**, the discharge times were obtained at 17, 19, 46, and 50 seconds in 3.0 M KCl electrolyte solution, respectively. Figure 3c shows the values of gravimetric capacitances obtained from cyclic voltammograms and galvanostatic charge-discharge experiments. At a scan rate of 100 mV s^{-1}, the capacitance values for the PANI, PANI/AY17, PANI/MWCNTs, and PANI/MWCNT/AY17-3 were determined to be 55.0, 90.3, 151.1, and 177.9 F g^{-1}, respectively. At 8.3 current density, the capacitance values obtained from the GCD test were 109.0, 121.8, 301.3, and 320.5 F g^{-1} for PANI, PANI/AY17, PANI/MWCNTs, and PANI/MWCNT/AY17-3, respectively. When MWCNTs were added to PANI, the composite's specific capacitance rose when compared to PANI. According to the results of the BET surface area analysis, this leads to improved pore accessibility for electrode/electrolyte ion exchange. In addition, the functional groups of the AY17 dye enabled the development of redox behaviour of the PANI. In addition, -Cl bonds, N-N bonds in the ring structure, and sulfonate groups (SO_3^-) in the AY17 dye structure strengthened the delocalization in the chain structure, supporting the redox behavior of PANI (36).

PANI, PANI/AY17, PANI/MWCNTs, and PANI/MWCNT/AY17-3 electrode Nyquist curves fitted to a simple circuit model are shown in Figure 3d (inset in **Figure 3d**). Table 3 shows the impedance values of Rs, Rct, Cdl, and W obtained after fitting according to the simple circuit model. The results generated from the EIS analysis have error rates of less than 5%. The PANI/MWCNT/AY17-3 electrode had the lowest Rs value, while the PANI electrode showed the highest Rs value. The Rs values of PANI, PANI/AY17, PANI/MWCNTs, and PANI/MWCNT/AY17-3 electrodes were determined as 3.978 Ω, 3.458 Ω, 3.412 Ω, and 2.825 Ω, respectively. It caused a decrease in Rs and Rct values thanks to functional groups such as sulfonyl groups in the AY17 structure, which were added as counter-ions to the chain structure of PANI. In addition, Rs and Rct values were lower in the PANI/MWCNT/AY17-3 electrode since the benzenoid structure of PANI was supported by MWCNTs added to the medium during hydrothermal synthesis. The Rct values of PANI, PANI/AY17, PANI/MWCNTs, and PANI/MWCNT/AY17-3 electrodes were determined as 4.337 Ω, 4.171 Ω, 3.885 Ω, and 3.247 Ω, respectively. Small differences between Rs and Rct values were as expected since the EIS analyses of the electrodes were performed in the same electrolyte. The highest Cdl value was 577.4 e-6, and it belonged to the PANI/MWCNT/AY17-3 electrode synthesized together with AY17, and MWCNTs added to the medium during PANI synthesis. MWCNT, which improved the chain structure of PANI and caused an increase in delocalization in the benzenoid structure of PANI thanks to its strong electronic structure, caused the Rs and Rct to be lower in the PANI/MWCNT/AY17-3 electrode than the other electrodes and increased the Cdl value. Warburg impedance values (W) were determined as 308.8 e-6, 333.6 e-6, 476.7 e-6, and 553.5 e-6 for PANI, PANI/AY17, PANI/MWCNTs, and PANI/MWCNT/AY17-3 electrodes, respectively. The results obtained in the EIS analyses were also in agreement with the results of the CV and GCD analyzes of the electrodes. Here, the functional groups in the AY17 dye enabled the development of the PANI structure, while the MWCNTs added to the medium with AY17 reduced the resistance values of PANI, allowing the potential operating range to expand and displaying a more stable charge-discharge feature.

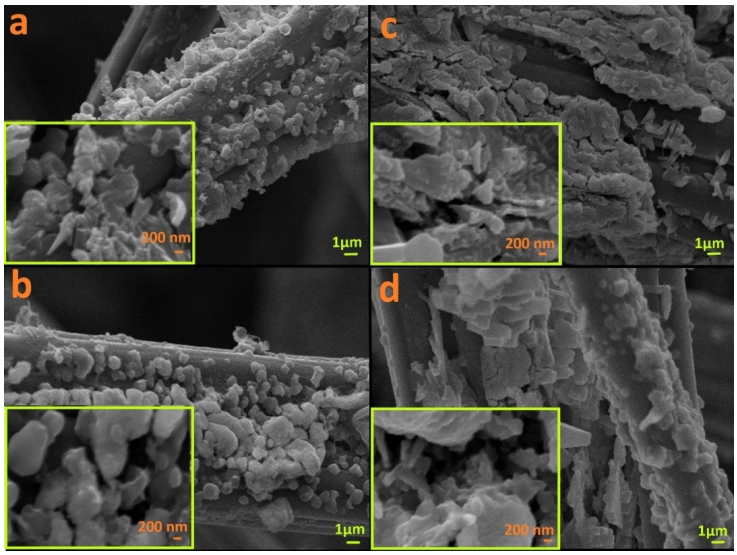

Figure 2: The SEM images of a) PANI, b) PANI/AY17, c) PANI/MWCNTs and d) PANI/MWCNT/AY17-3 electrode surfaces.

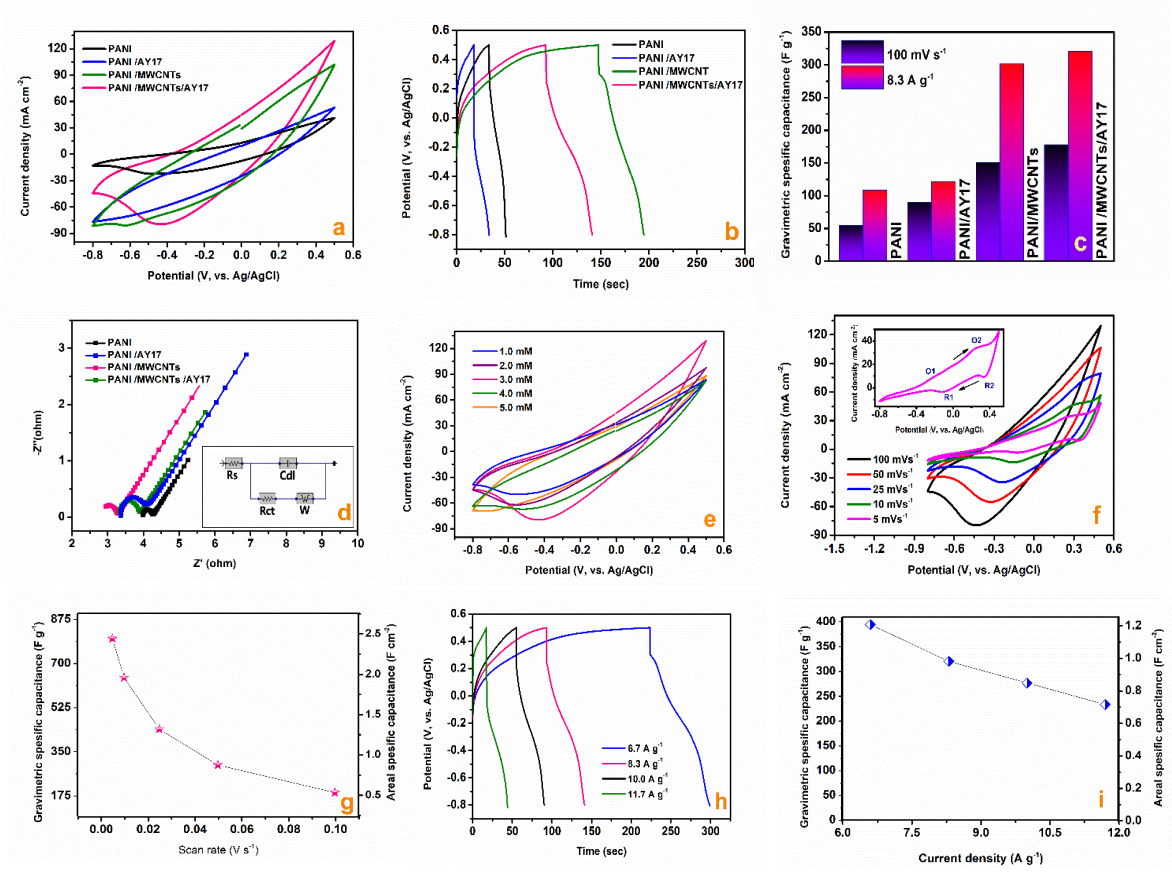

Figure 3: a) CVs at 100 mV s-1, b) GCD curves at 8.3 A g-1, c) Specific capacitance from CVs and GCD test, d) EIS Nyquist curves, the inset is equivalent circuit model, e) Effect of AY17 concentration on PANI/MWCNTs composite electrode, f) CV measurements of the PANI/MWCNT/AY17-3 electrode at different scan rates, g) Specific capacitance from CVs of the PANI/MWCNT/AY17-3 electrode, h) GCD profiles of the PANI/MWCNT/AY17-3 electrode at different current densities, i) Specific capacitance from GCD test of the PANI/MWCNT/AY17-3 electrode.

Table 3: Fitted impedance values of PANI, PANI/AY17, PANI/MWCNTs and PANI/MWCNT/AY17-3 electrodes.

Electrode Material	Rs / Ω	Rct / Ω	Cdl / F	W
PANI	3.978	4.337	245.1 e^{-6}	308.8 e^{-6}
PANI/AY17	3.548	4.171	417.5 e^{-6}	333.6 e^{-6}
PANI/MWCNTs	3.412	3.885	395.6 e^{-6}	476.7 e^{-6}
PANI/MWCNTs/AY17-3	2.825	3.247	577.4 e^{-6}	535.5 e^{-6}

In **Figure 3e**, the effect of different acid yellow 17 dye concentrations on the supercapacitor electrode of PANI/MWCNT on the flexible carbon felt was investigated using a half-cell system in 3.0 M KCl electrolyte solution, −0.8 V-(0.5) V vs Ag/AgCl operating potential window. An increase in the encircled area was observed in the CV of PANI/MWCNTs/AY17-3, indicating that the redox-active surface area at the electrode surface was more accessible (37,38). As a result, greater ion interaction at the electrolyte and electrode interface was found to improve charge storage performance.

The behavior of PANI/MWCNTs/AY17-3 supercapacitor electrodes at various scan rates of 5, 10, 20, 30, 50, and 100 mVs^{-1} was given in **Figure 3f.** The composite electrode showed two double redox peaks (-0.20/-0.11V and ~0.27/0.35V) at the scan rate of 5 mVs^{-1}. The conversion of the totally reduced leucoemeraldine base to partially oxidized emeraldine was linked with the first set of redox peaks, whereas the conversion of emeraldine to the fully oxidized pernigraniline form was related with the second set of redox peaks. (39). In **Figure 5g**, the value of specific capacitances was 814.1, 653.2, 439.8, 292.0, and 177.9 F g^{-1} at scan rates of 5 to 100 mV s^{-1}, respectively, calculated by the cyclic voltammograms from **Figure 5f**. This result showed that the PANI/MWCNTs/AY17-3 electrode has an excellent charge transfer process for energy storage systems. The charge-discharge profiles of the supercapacitor electrode were tested at various current densities of 6.6, 8.3, 10.0, and 11.7 Ag^{-1} in **Figure 3h**. The gravimetric and areal-specific capacitances of GCD test were presented in **Figure 3i**. The specific capacitances obtain at 394.9, 320.5, 276.9, and 233.3 F g^{-1} at the current densities of 6.6, 8.3, 10.0 and 11.7 Ag^{-1}, respectively. When we compared the SEM images of PANI and PANI/MWCNTs/AY17-3 electrode shown in **Figure 2**, the compactness and regular morphology of the PANI/MWCNTs/AY17-3 coated on a carbon felt surface was superior to the electrode made with PANI. Furthermore, when the surface area and pore volume features of PANI/MWCNTs/AY17-3 and other electrodes were examined using the N_2 adsorption-desorption isotherms displayed in **Figure 1d**, the increase in electrode surface and electrochemical behavior were found to be consistent with the results. The morphology and electrochemical behavior of the PANI/MWCNTs/AY17-3 may be resulted from the electron-rich structure of disodium 2,5-dichloro-4-(5-hydroxy-3-methyl-4-(sulfophenylazo) pyrazol-1-yl) benzenesulfonate. Azo compounds enable electron delocalization as they contain both the benzene rings and the two nitrogen atoms connecting the rings (40). The presence of electron withdrawing and electron donating electrons can be very attractive for the use of these materials in textile-based energy storage studies. It also contains sulfonic groups with high protonation degree and electrical conductivity properties, which improves the capacitive property of the electrode. **Table 4** shows a literature search of capacitance values and other supercapacitor parameters using PANI polymer as the supercapacitor electrode.

The PANI/MWCNTs/AY17-3 electrode was used to build a symmetric supercapacitor device (full cell). Figures 4 and 5 illustrate the cell's electrochemical and capacitive performance in an aqueous 3.0 M KCl electrolyte solution (a-d). Figure 4a depicted the symmetric supercapacitor's cyclic voltammogram at various scan rates ranging from 5 to 200 mV s^{-1}. The operating potential of the supercapacitor was regulated between 0 and 0.9 V. Despite the higher scan rates, CV regions in cyclic voltammograms showed some coherence, depending on the scan rate. Figure 4b shows the gravimetric specific capacitance values calculated from the cyclic voltammograms in Figure 4a using Eq (1). As the scan rate ranged from 5-100 mV s^{-1}, the capacitance value fluctuated from 127.9 to 45.0 F g^{-1}. Figure 4c depicts charge–discharge testing at various current densities ranging from 0.3 to 2.0 A g^{-1}. The device's gravimetric specific capacitance value was estimated using the GCD test and Eq (2). In Figure 4d, the specific capacitance decreases from 103.7 to 40.0 F g^{-1} as the current density increases from 0.3 to 2.0 A g-1. At current densities of 0.3, 0.6, 1.0, 1.3, 1.7, and 2.0 A g^{-1}, IR drop values of 0.03, 0.05, 0.07, 0.09, 0.14, and 0.15 V were obtained from discharge curves at various current densities. In the galvanostatic discharge test, the electrode

retained 78.57 percent of its capacitance in the current density range of 0.3 to 1.7 A g^{-1}, indicating excellent charge transfer and high capacitance.

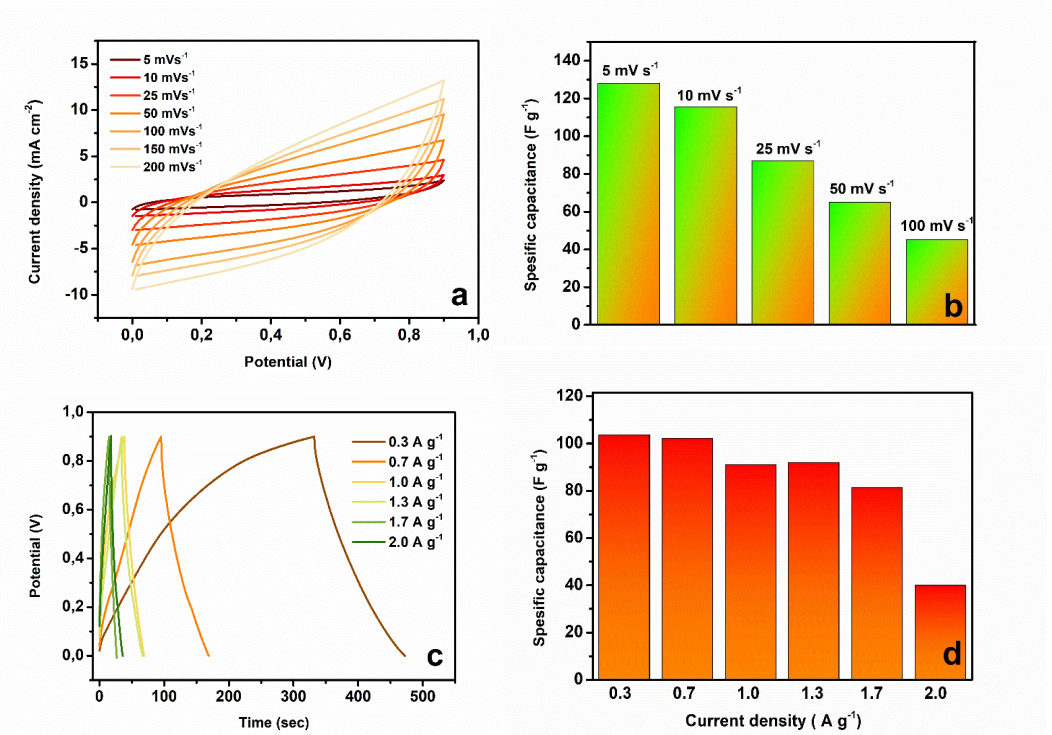

Figure 4: a) CVs at different scan rates, b) Specific capacitance values from CVs, c) GCD curves at different current densities, d) Specific capacitance values from GCD of symmetric supercapacitor.

Figure 5a shows a long-life cycling test of a symmetric supercapacitor. The capacitance retention of a symmetric supercapacitor was tested through 2,500 CV cycles at a scan rate of 200 mV s^{-1} with a potential window of 0.9 V. Despite using only polymeric and low-cost components and an aqueous electrolyte, the device demonstrated good capacitance retention of 81.76 percent after 2,500 cycles. As the number of cycles increased, the capacitance value decreased, indicating that sections of the electrode surface were no longer accessible to electrolyte ions.

Figure 5b shows the Nyquist curves obtained as a result of the EIS analysis of the PANI//MWCNTs/AY17-3 // PANI//MWCNTs/AY17-3 symmetric supercapacitor before the long cycle test and after 2,500 cycles. The equivalent circuit model was presented in the inset of **Figure 5b**. While the Cdl value of the symmetrical supercapacitor device was 396.5 e^{-6} before charge-discharge, it decreased to 289.4 e^{-6} after 2500 cycles, as expected. According to the Cdl values, after 2,500 cycles, the PANI//MWCNTs/AY17-3 // PANI//MWCNTs/AY17-3 symmetric supercapacitor largely preserved its capacitance. The Warburg impedance value was initially 417.9 e^{-6}. After 2500 cycles, this value became 356.4 e^{-6}. The decrease in the Warburg impedance value was caused by partial deformation due to ion adsorption on the electrode surface over time after the long cycle test. The difference between the Rs and Rct values of the symmetric supercapacitor device before the long cycle test was lower than the difference between the Rs and Rct values after 2500 cycles. After 2500 cycles, the charge transfer resistance increased as the ions adsorbed on the electrode surface and the redox active regions reduced.

Table 4: The list of the maximum capacitance, electrolyte, and capacitance retention tests for PANI-based electrodes materials and devices**.**

Electrode materials	Electrolyte	Measurement type	Max. Capacitance	Cycling	Method	Ref
PANI/MWCNT	0.5 M H_2SO_4	3-electrode	590.7 F g^{-1} **,** 50 mVs^{-1}	500 (90%)	Chemical synthesis	(41)
PANI/MWCNTs (8 wt%)	PVA/H_2SO_4,	3-electrode	446.9 F g^{-1}, 40 mVs^{-1}	10,000 (84%)	Chemical synthesis	(42)
PANI/MWNTs	1.0 M $NaNO_3$	3-electrode	328 F g^{-1}, 5 mA cm^{-2}	1,000 (80%)	CVD/ Chemical synthesis	(43)
PANI/CNT	-	3-electrode	1266 F g^{-1}, 1 A g^{-1}	10,000 (83%)	Chemical grafting polymerization	(44)
PANI/MWCNT	1.0 M $LiClO_4$	3-electrode	174 F g^{-1}, 0.5 A g^{-1}	1,000 (100%)	Chemical synthesis	(45)
PANI/MWCNT	1.0 M H_2SO_4 PVA/H_2SO_4/ NQS	3-electrode 2-electrode	1100 F g^{-1}, 5 mVs^{-1} -	3,000 (93%)	Enzymatic synthesis	(46)
GNS/PANI	1.0 M H_2SO_4	3-electrode	532.3 F g^{-1} ,2 mVs^{-1}	1,000 (99%)	Hydrothermal synthesis	(20)
Graphene/MnO2/PANI	1.0 M Na_2SO_4	3-electrode	305 F g-1 , 1 A g^{-1}	1,000 (90%)	Hydrothermal synthesis	(47)
PC-Cs/CNTs/PANI	6.0 M KOH	3-electrode 2-electrode	767 F g^{-1} , 1 A g^{-1} 102.5 F g^{-1},0.5 A g^{-1}	5,000 (88%)	Chemical synthesis	(48)
PANI//MWCNTs/AY17-3	3.0 M KCl	3-electrode 2-electrode	814.1 F g^{-1}**,** 5 mVs^{-1} 127 F g^{-1}**,** 5 mVs^{-1}	2,500 (82%)	Hydrothermal synthesis	[This work]

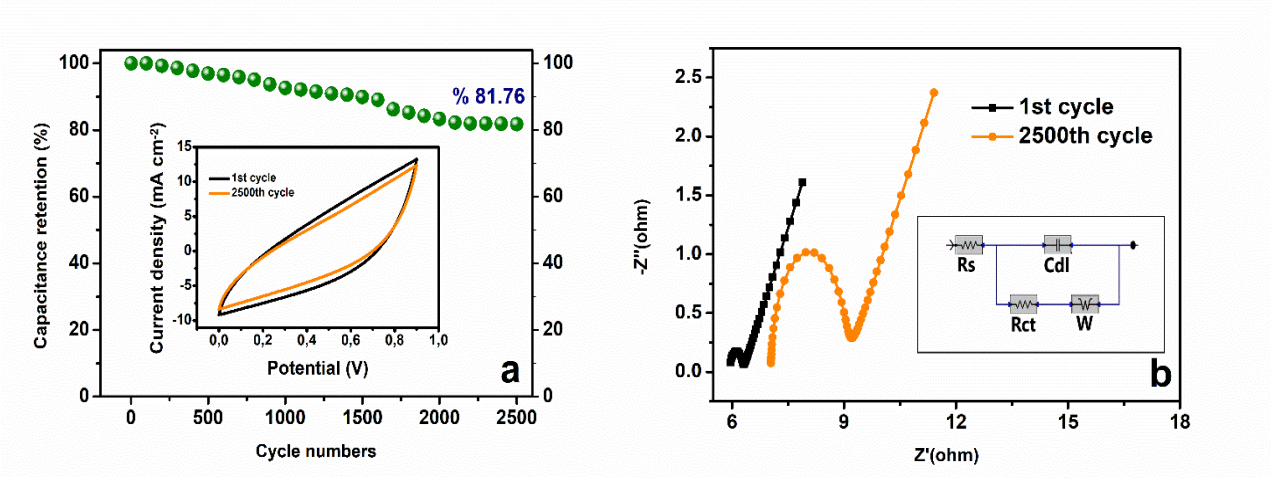

Figure 5: a) Long life cycling test of symmetric supercapacitor, b) Nyquist impedance curves of symmetric supercapacitor. The inset is equivalent circuit model.

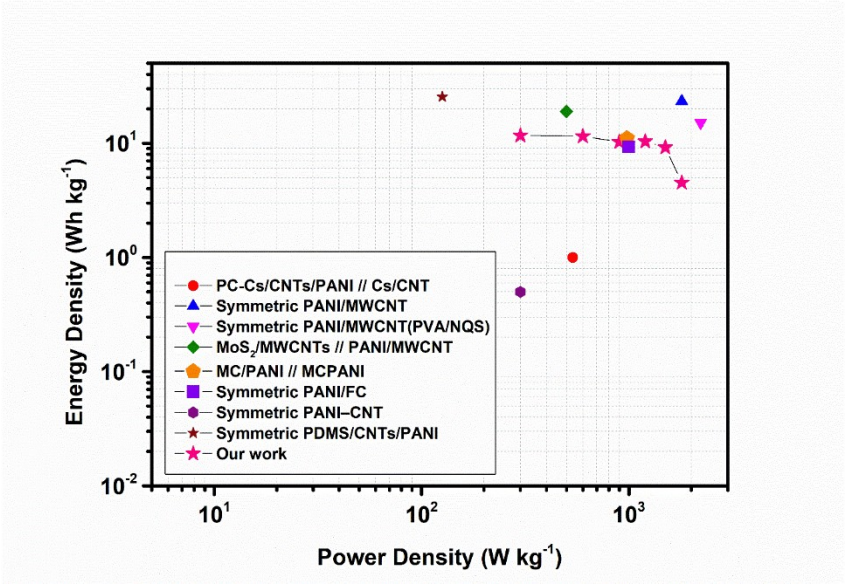

Figure 6: Energy density and power density for comparing our supercapacitor in Ragone plot.

According to Equations (3) and (4), the symmetric supercapacitor had a maximum energy density of 11.7 Wh/kg at 0.3 A g^{-1} and a maximum power density of 1800 W/kg at 2.0 A g^{-1} (4). Figure 5 shows that the built symmetrical supercapacitor had a good energy and power density range when compared to the literature. The device's Ragone plot is based on the GCD test. In the asymmetrical supercapacitor made utilizing PC-Cs/CNTs/PANI as the positive electrode and PC-Cs/CNT as the negative electrode, the device had an energy density of 56.9 Wh kg^{-1} at a power density of 537 W kg^{-1}, which was higher than some previously reported PANI-based supercapacitors (48). At a high power density of 2217.95 W/kg, the MoS_2|MWCNTs and PANI|MWCNTs composite electrodes had an energy density of 15.09 Wh/kg (49). At 0.5 $kWkg^{-1}$, the complete symmetric cell made of MC/PANI has a high energy density of 19 $Whkg^{-1}$. (50). For PANI/MWCNT, energy density and power density for the device were calculated as 11.1 Wh/kg and 0.98 kW/kg (51). The maximum specific energy of 0.5 Wh kg^{-1} and a maximum specific power of 0.3 kW kg^{-1}, were found for PANI–CNT flexible supercapacitors (52).

CONCLUSIONS

PANI//MWCNTs/AY17-3 composite electrode was successfully synthesized by hydrothermal synthesis, and its supercapacitor performance was investigated via electrochemical characterizations. By altering the dye content of AY17, the behavior of AY17 in modulating electrochemical

characteristics of PANI/CNT composite was investigated. At a scan rate of 5 mV s^{-1}, the PANI/MWCNTs/AY17 composite electrode with 3mM AY17 demonstrated a maximum specific capacitance of 814.1 F g^{-1}, which was much greater than PANI and PANI/MWCNTs composite electrodes. In a 3.0 M KCl aqueous electrolyte, a symmetric supercapacitor has a maximum energy density of 11.7 W h kg^{-1} and a maximum power density of 1800 W kg^{-1}. After 2000 cycles, the capacitance retention of the symmetric supercapacitor was determined to be greater than 80%. The influence of a textile dye on a multi-walled carbon nanotubes/polyaniline composite as a promising supercapacitor electrode material for next-generation textile-based flexible supercapacitors was supported by all of the findings.

REFERENCES

1. Chakraborty S, L. MN. Review{\textemdash}An Overview on Supercapacitors and Its Applications. J Electrochem Soc [Internet]. 2022;169(2):20552. Available from: <URL>.

2. Mohd Abdah MAA, Azman NHN, Kulandaivalu S, Sulaiman Y. Review of the use of transition-metal-oxide and conducting polymer-based fibres for high-performance supercapacitors. Mater Des. 2019;186:108199. <URL>.

3. Yazar S, Arvas MB, Sahin Y. An ultrahigh-energy density and wide potential window aqueous electrolyte supercapacitor built by polypyrrole/aniline 2-sulfonic acid modified carbon felt electrode. Int J Energy Res [Internet]. Available from: <URL>.

4. Uke SJ, Mardikar SP, Kumar A, Kumar Y, Gupta M, Kumar Y. A review of π-conjugated polymer-based nanocomposites for metal-ion batteries and supercapacitors. R Soc Open Sci. 2021;8(10). <URL>.

5. Arvas MB, Gencten M, Sahin Y. One-step synthesized N-doped graphene-based electrode materials for supercapacitor applications. Ionics (Kiel). 2021 May;27(5):2241–56. <URL>.

6. Arvas MB, Yazar S, Sahin Y. Electrochemical synthesis and characterization of self-doped aniline 2-sulfonic acid-modified flexible electrode with high areal capacitance and rate capability for supercapacitors. Synth Met [Internet]. 2022;285:117017. Available from: <URL>.

7. Liao G, Gong Y, Yi C, Xu Z. Soluble, Antibaterial, and Anticorrosion Studies of Sulfonated Polystyrene/Polyaniline/Silver Nanocomposites Prepared with the Sulfonated Polystyrene Template. Chinese J Chem [Internet]. 2017;35(7):1157–64. Available from: <URL>.

8. Beygisangchin M, Abdul Rashid S, Shafie S, Sadrolhosseini AR, Lim HN. Preparations, Properties, and Applications of Polyaniline and Polyaniline Thin Films-A Review. Polymers (Basel) [Internet]. 2021 Jun 18;13(12):2003. Available from: <URL>.

9. Thakur AK, Choudhary RB, Majumder M, Majhi M. Fairly improved pseudocapacitance of PTP/PANI/TiO2 nanohybrid composite electrode material for supercapacitor applications. Ionics (Kiel) [Internet]. 2018;24(1):257–68. Available from: <URL>.

10. Thakur AK, Deshmukh AB, Choudhary RB, Karbhal I, Majumder M, Shelke M V. Facile synthesis and electrochemical evaluation of PANI/CNT/MoS2 ternary composite as an electrode material for high performance supercapacitor. Mater Sci Eng B [Internet]. 2017;223:24–34. Available from: <URL>.

11. Dawouda HD, Altahtamounia TM, Zaghoa MM, Bensalahb N. A brief overview of flexible CNT/PANI super capacitors. Mater Sci Nanotechnol. 2017;01(02).

12. Li J, Qiu S, Liu B, Chen H, Xiao D, Li H. Strong interaction between polyaniline and carbon fibers for flexible supercapacitor electrode materials. J Power Sources [Internet]. 2021;483(August 2020):229219. Available from: <URL>.

13. Lü QF, Chen G, Lin TT, Yu Y. Dye-functionalized graphene/polyaniline nanocomposite as an electrode for efficient electrochemical supercapacitor. Compos Sci Technol [Internet]. 2015;115:80–6. Available from: <URL>.

14. Wang Q, Song H, Li W, Wang S, Liu L, Li T, et al. Facile synthesis of polypyrrole/graphene composite aerogel with Alizarin Red S as reactive dopant for high-performance flexible supercapacitor. J Power Sources [Internet]. 2022;517:230737. Available from: <URL>.

15. Xueying Y, Jijue L, Xinkun S, Yingzhao H, Xiaoxiao D, Yongjin Z, et al. Facile Synthesis of Polyaniline-Prussian Blue Composite for High-Performance Supercapacitors. Int J Nanoparticles Nanotechnol. 2017;3(1).

16. Arvas MB, Gürsu H, Gencten M, Sahin Y. Preparation of different heteroatom doped graphene oxide based electrodes by electrochemical method and their supercapacitor applications. J Energy Storage [Internet]. 2021 Mar;35:102328. Available from: <URL>.

17. Wang Q, Feng Y, Feng J, Li D. Enhanced thermal- and photo-stability of acid yellow 17 by incorporation into layered double hydroxides. J Solid State Chem [Internet]. 2011;184(6):1551–5. Available from: <URL>.

18. Jin L, Jiang Y, Zhang M, Li H, Xiao L, Li M, et al. Oriented Polyaniline Nanowire Arrays Grown on Dendrimer (PAMAM) Functionalized Multiwalled Carbon Nanotubes as Supercapacitor Electrode Materials. Sci Rep [Internet]. 2018;8(1):6268. Available from: <URL>.

19. Yasuda A, Shimidzu T. Chemical Oxidative Polymerization of Aniline with Ferric Chloride. 1993;25(4):329–38. <URL>.

20. Wang R, Han M, Zhao Q, Ren Z, Guo X, Xu C, et al. Hydrothermal synthesis of nanostructured graphene/polyaniline composites as high-capacitance electrode materials for supercapacitors. Sci Rep

[Internet]. 2017;7(1):44562. Available from: <URL>.

21. Pandey K, Yadav P, Mukhopadhyay I. Elucidating the effect of copper as a redox additive and dopant on the performance of a PANI based supercapacitor. Phys Chem Chem Phys. 2015;17(2):878–87. <URL>.

22. Lim SP, Huang NM, Lim HN. Solvothermal synthesis of SnO2/graphene nanocomposites for supercapacitor application. Ceram Int [Internet]. 2013;39(6):6647–55. Available from: <URL>.

23. Sajjad M, Chen X, Yu C, Guan L, Zhang S, Ren Y, et al. High Energy Density Asymmetric Supercapacitor Based on NiCo2S4/CNTs Hybrid and Carbon Nanotube Paper Electrodes. J Mol Eng Mater [Internet]. 2019;07(01n02):1950004. Available from: <URL>.

24. Qiu G, Zhu A, Zhang C. Hierarchically structured carbon nanotube-polyaniline nanobrushes for corrosion protection over a wide pH range. RSC Adv. 2017;7(56):35330–9. <URL>.

25. John A, Mahadeva SK, Kim J. The preparation, characterization and actuation behavior of polyaniline and cellulose blended electro-active paper. Smart Mater Struct. 2010;19(4). <URL>.

26. Padmapriya S, Harinipriya S, Jaidev K, Sudha V, Kumar D, Pal S. Storage and evolution of hydrogen in acidic medium by polyaniline. Int J Energy Res. 2018;42(3):1196–209. <URL>.

27. Iqbal J, Ansari MO, Numan A, Wageh S, Al-Ghamdi A, Alam MG, et al. Hydrothermally Assisted Synthesis of Porous Polyaniline@Carbon Nanotubes–Manganese Dioxide Ternary Composite for Potential Application in Supercapattery. Polymers (Basel) [Internet]. 2020;12(12). Available from: <URL>.

28. Mitra M, Kulsi C, Chatterjee K, Kargupta K, Ganguly S, Banerjee D, et al. Reduced graphene oxide-polyaniline composites—synthesis{,} characterization and optimization for thermoelectric applications. RSC Adv [Internet]. 2015;5(39):31039–48. Available from: <URL>.

29. Tang L, Duan F, Chen M. Fabrication of ferric chloride doped polyaniline/multilayer super-short carbon nanotube nanocomposites for supercapacitor applications. J Solid State Electrochem. 2016;20. <URL>.

30. Rajagopalan B, Hur SH, Chung JS. Surfactant-treated graphene covered polyaniline nanowires for supercapacitor electrode. Nanoscale Res Lett [Internet]. 2015;10(1):1–9. Available from: <URL>.

31. Ali LIA, Ismail HK, Alesary HF, Aboul-Enein HY. A nanocomposite based on polyaniline, nickel and manganese oxides for dye removal from aqueous solutions. Int J Environ Sci Technol [Internet]. 2021;18(7):2031–50. Available from: <URL>.

32. Ahmad S, Sultan A, Raza W, Muneer M, Mohammad F. Boron nitride based polyaniline nanocomposite: Preparation, property, and application. J Appl Polym Sci. 2016;133(39). <URL>.

33. Bhat MA, Rather RA, Shalla AH. PEDOT and PEDOT:PSS conducting polymeric hydrogels: A report on their emerging applications. Synth Met [Internet]. 2021;273(January):116709. Available from: <URL>.

34. Hilário RB, de Moraes TH, da Rocha Pimentel Gonçalves JM, Gandara M, Gonçalves ES. Influence of heat treatment and electrochemical treatment on the properties of PANI electrodeposited on carbon fiber felt. Diam Relat Mater [Internet]. 2022;123:108867. Available from: <URL>.

35. Ibrahim NI, Wasfi AS. Electrochemical evaluation of polyaniline/multi-walled carbon nanotube composite synthesized by microwave plasma polymerization as a supercapacitor electrode. IOP Conf Ser Mater Sci Eng. 2020;757(1). <URL>.

36. Yazar S, Atun G. Electrochemical synthesis of tunable polypyrrole-based composites on carbon fabric for wide potential window aqueous supercapacitor. Int J Energy Res [Internet]. Available from: <URL>.

37. Rincón RA, Artyushkova K, Mojica M, Germain MN, Minteer SD, Atanassov P. Structure and Electrochemical Properties of Electrocatalysts for NADH Oxidation. Electroanalysis [Internet]. 2010;22(7–8):799–806. Available from: <URL>.

38. Jarjes ZA, Samian MR, Ab Ghani S. Conductive polymers: Their preparations and catalyses on NADH oxidation at carbon cloth electrodes. Arab J Chem [Internet]. 2015;8(5):726–31. Available from: <URL>.

39. Song E, Choi J-W. Conducting Polyaniline Nanowire and Its Applications in Chemiresistive Sensing. Nanomaterials. 2013;3:498–523. <URL>.

40. Li Y, Patrick BO, Dolphin D. Near-Infrared Absorbing Azo Dyes: Synthesis and X-ray Crystallographic and Spectral Characterization of Monoazopyrroles, Bisazopyrroles, and a Boron−Azopyrrole Complex. J Org Chem [Internet]. 2009 Aug 7;74(15):5237–43. Available from: <URL>.

41. Ates M, Serin MA, Calisskan S. Electrochemical supercapacitors of PANI/MWCNT, PEDOT/MWCNT and P(ANI-co-EDOT)/MWCNT nanocomposites. Polym Bull [Internet]. 2019 Jun 27;76(6):3207–31. Available from: <URL>.

42. Pal R, Goyal SL, Rawal I. High-performance solid state supercapacitors based on intrinsically conducting polyaniline/MWCNTs composite electrodes. J Polym Res [Internet]. 2020;27(7):179. Available from: <URL>.

43. Dong B, He B-L, Xu C-L, Li H-L. Preparation and electrochemical characterization of polyaniline/multi-walled carbon nanotubes composites for supercapacitor. Mater Sci Eng B [Internet]. 2007;143(1):7–13. Available from: <URL>.

44. Che B, Li H, Zhou D, Zhang Y, Zeng Z, Zhao C, et al. Porous polyaniline/carbon nanotube composite electrode for supercapacitors with outstanding rate capability and cyclic stability. Compos Part B Eng [Internet]. 2019;165:671–8. Available from: <URL>.

45. M. J, M. M, Jayalekshmi S, Jayaraj MK. PANI/MWCNT composite electrode for supercapacitor

applications. In: Kobayashi NP, Talin AA, Islam MS, Davydov A V, editors. Low-Dimensional Materials and Devices 2018 [Internet]. SPIE; 2018. p. 33–8. Available from: <URL>.

46. Shumakovich GP, Morozova O V, Khlupova ME, Vasil'eva IS, Zaitseva EA, Yaropolov AI. Enhanced performance of a flexible supercapacitor due to a combination of the pseudocapacitances of both a PANI/MWCNT composite electrode and a gel polymer redox electrolyte. RSC Adv [Internet]. 2017;7(54):34192–6. Available from: <URL>.

47. Chen W, Tao X, Li Y, Wang H, Wei D, Ban C. Hydrothermal synthesis of graphene-MnO2-polyaniline composite and its electrochemical performance. J Mater Sci Mater Electron. 2016;27(7):6816–22. <URL>.

48. Hong X, Wang X, Li Y, Deng C, Liang B. Potassium citrate-derived carbon nanosheets/carbon nanotubes/polyaniline ternary composite for supercapacitor electrodes. Electrochim Acta [Internet]. 2022;403:139571. Available from: <URL>.

49. Cheng B, Cheng R, Tan F, Liu X, Huo J, Yue G. Highly Efficient Quasi-Solid-State Asymmetric Supercapacitors Based on MoS2/MWCNT and PANI/MWCNT Composite Electrodes. Nanoscale Res Lett [Internet]. 2019;14(1):66. Available from: <URL>.

50. Banerjee J, Dutta K, Kader MA, Nayak SK. An overview on the recent developments in polyaniline-based supercapacitors. Polym Adv Technol [Internet]. 2019;30(8):1902–21. Available from: <URL>.

51. Malik R, Zhang L, McConnell C, Schott M, Hsieh Y-Y, Noga R, et al. Three-dimensional, free-standing polyaniline/carbon nanotube composite-based electrode for high-performance supercapacitors. Carbon N Y [Internet]. 2017;116:579–90. Available from: <URL>.

52. Liu Q, Nayfeh MH, Yau S-T. Brushed-on flexible supercapacitor sheets using a nanocomposite of polyaniline and carbon nanotubes. J Power Sources [Internet]. 2010;195(21):7480–3. Available from: <URL>.